Sensor signal processing

Complex Number Assignment in the Topology Method for Heartbeat Interval Estimation Using Millimeter-Wave Radar

Yuji Tanaka* [ID], Kimitaka Sumi [ID], Itsuki Iwata** [ID], and Takuya Sakamoto*** [ID]

Department of Electrical Engineering, Graduate School of Engineering, Kyoto University, Kyoto 615-8510, Japan
*Member, IEEE*
**Graduate Student Member, IEEE*
***Senior Member, IEEE*

Abstract—The topology method is an algorithm for accurate estimation of instantaneous heartbeat intervals using millimeter-wave radar signals. In this model, feature points are extracted from the skin displacement waveforms generated by heartbeats, and a complex number is assigned to each feature point. However, these numbers have been assigned empirically and without solid justification. This letter used a simplified model of displacement waveforms to predict the optimal choice of the complex number assignments to feature points corresponding to inflection points, and the validity of these numbers was confirmed using analysis of a publicly available dataset.
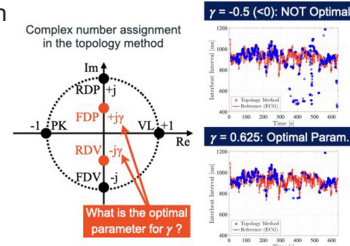
Index Terms—Sensor signal processing, interbeat interval (IBI), millimeter-wave, noncontact sensing, physiological signals, topology method.

I. INTRODUCTION

Global population aging creates a high demand for continuous monitoring of physiological signals [1]. Among these, heart rate is particularly important for monitoring health status and detecting signs of cardiovascular disease. In addition, heart rate variability can be used to capture emotional changes [2], [3] and monitor mental state [4]. The most common methods for monitoring heart rate are electrocardiography and photoplethysmography. These use contact-type sensors that can cause discomfort and restrict the wearer's activities [5] and are therefore unsuitable for long-term monitoring applications. In contrast, radar-based methods that measure body surface displacement caused by heart motion and pulse waves have attracted attention because they enable long-term heartbeat monitoring without sensor attachment [6], [7], [8], [9], [10].

The topology method [11] is an accurate technique for estimating the instantaneous heartbeat interval using radar signals and has found various applications, such as autonomic nervous system activity estimation [12], camera-based heart rate estimation [13], and animal monitoring [14]. In the topology method, several feature points are extracted from the skin displacement waveform caused by heartbeats, and a complex number is assigned to each of the feature points. However, studies to date have set these numbers empirically, and thus, the question of how to validate the complex number assignments remains open. In this letter, we used a simplified model of the displacement waveform to quantitatively evaluate the validity of the complex numbers assigned to feature points corresponding to two types of inflection points, and we analyzed its performance. A preprint of this manuscript has been posted [15].

Table 1. Comparison of the IBI Estimation Accuracy Between the Topology Method and Other Methods

	Wang et al. [9]	Chen et al. [10]	Iwata et al. [14]
Method	VMD	DNN	Topology + HPF
Radar type	FMCW	FMCW	FMCW
Center frequency	79 GHz	79 GHz	79 GHz
RMS error	26 ms	3 ms	2.55 ms

VMD: variational mode decomposition, DNN: deep neural network,
HPF: high-pass filter, FMCW: frequency-modulated continuous-wave,
RMS: root mean square

II. TOPOLOGY METHOD

The topology method [11] can accurately estimate the interbeat interval (IBI) of the heart by using topology correlation coefficients calculated from the complex numbers assigned to the extracted feature points in combination with ordinary correlation coefficients. As given in Table 1, it is reported that the topology method achieves high accuracy in estimating IBI in comparison with other representative studies [9], [10]. The topology method extracts the following six types of feature points from the displacement waveform $s(t)$.

1) Peak (PK): $\dot{s}(t) = 0$, $\ddot{s}(t) < 0$;
2) Valley (VL): $\dot{s}(t) = 0$, $\ddot{s}(t) > 0$;
3) Rising derivative peak (RDP): $\dot{s}(t) > 0$, $\ddot{s}(t) = 0$, $\dddot{s}(t) < 0$;
4) Rising derivative valley (RDV): $\dot{s}(t) > 0$, $\ddot{s}(t) = 0$, $\dddot{s}(t) > 0$;
5) Falling derivative peak (FDP): $\dot{s}(t) < 0$, $\ddot{s}(t) = 0$, $\dddot{s}(t) < 0$;
6) Falling derivative valley (FDV): $\dot{s}(t) < 0$, $\ddot{s}(t) = 0$, $\dddot{s}(t) > 0$.

To estimate the IBI, the topology method detects pairs of feature points of the same type that have high topology and ordinary correlation coefficients.

First, the ordinary correlation coefficients are calculated. Let τ_n be the time of the nth feature point extracted from $s(t)$. The $(2K + 1)$-dimensional vector, $\overline{\boldsymbol{v}}_n$, composed of the signal samples around the
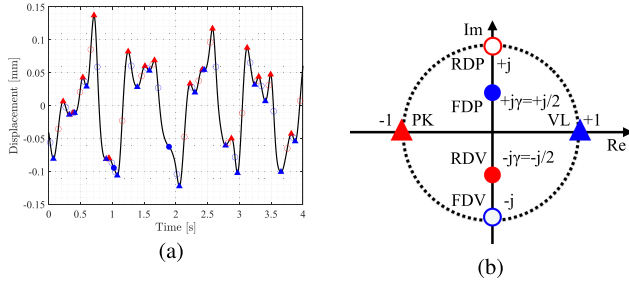
Fig. 1. Complex values assigned to feature points from which the topology correlation values are calculated. (a) Example of the displacement waveform $s(t)$. (b) Feature points.

nth feature point is expressed as $\overline{\boldsymbol{v}}_n = [s(\tau_n - K\Delta t), s(\tau_n - (K - 1)\Delta t), \ldots, s(\tau_n + K\Delta t)]^{\mathsf{T}}$, where Δt is the sampling interval, K is a parameter determined by $K\Delta t = T_c/2$, T_c is the time width used to calculate an ordinary correlation coefficient, and the superscript T denotes the matrix transpose. Let $\boldsymbol{v}_n$ be the vector obtained by removing the DC component from $\overline{\boldsymbol{v}}_n$. The ordinary correlation between mth and nth feature points is then given by the coefficient $c_{m,n} = \boldsymbol{v}_m^{\mathsf{T}}\boldsymbol{v}_n/|\boldsymbol{v}_m||\boldsymbol{v}_n|$.

Next, the topology correlation coefficients are calculated. In the topology method, the complex numbers -1, 1, j, $-\mathrm{j}\gamma$, $\mathrm{j}\gamma$, and $-\mathrm{j}$ are assigned to the feature points PK, VL, RDP, RDV, FDP, and FDV, respectively, where $\gamma = 1/2$ and $\mathrm{j} = \sqrt{-1}$ is an imaginary unit (see Fig. 1). Each symbol shown in Fig. 1(a) corresponds to the same symbol shown in Fig. 1(b). Based on these assignments, the complex signal $s_t(t)$ is calculated by referring to the nearest feature point at time t. To obtain the topology correlation coefficient from $s_t(t)$, define a $(2K_t + 1)$-dimensional complex vector $\boldsymbol{u}_n$ for the nth feature point as $\boldsymbol{u}_n = [s_t(\tau_n - K_t\Delta t), s_t(\tau_n - (K_t - 1)\Delta t), \ldots, s_t(\tau_n + K_t\Delta t)]^{\mathsf{T}}$, where K_t is a parameter determined by $K_t\Delta t = T_t/2$, and T_t is the time width used to calculate the topology correlation values. The topology correlation $q_{m,n}$ between the mth and nth feature points is expressed as $q_{m,n} = |\boldsymbol{u}_m^{\mathsf{H}}\boldsymbol{u}_n|^2/|\boldsymbol{u}_m|^2|\boldsymbol{u}_n|^2$, where the superscript H denotes the complex conjugate of the matrix transpose. The set of feature points that satisfy both $c_{m,n} \geq c_{\mathrm{th}}$ and $q_{m,n} \geq q_{\mathrm{th}}$ are extracted, where c_{th} and q_{th} are thresholds for the ordinary correlation and the topology correlation coefficients, respectively. Finally, the IBI is estimated from the time difference between two adjacent feature points of the same type.

Note that the parameter $\gamma = 0.5$ is empirically set, so RDV and FDP, the feature points corresponding to inflection points, are empirically assigned the values $-\mathrm{j}/2$ and $\mathrm{j}/2$, respectively. Thus, the following factors should be considered. The first is the magnitude relationship between RDV and FDP. Considering that $\dot{s}(t) > 0$ for RDV and $\dot{s}(t) < 0$ for FDP, the number assigned to the imaginary part of RDV appears to exceed that assigned to FDP, but the actual relationship is opposite. In the original formulation of the topology method [11], this opposite assignment was shown to make the cross-correlation function steeper, but the effectiveness of such an assignment has not been verified quantitatively. The second factor is the magnitude of the assigned numbers. In the topology method, $\ddot{s}(t)$ and $\dot{s}(t)$ correspond to the real and imaginary parts of the complex number assignment, respectively. The only restriction imposed by the topology method on RDV and FDP, both of which satisfy $\ddot{s}(t) = 0$, is that the assigned numbers must be pure imaginary. The magnitudes of the coefficients for RDV and FDP do not necessarily satisfy $|\gamma| = 1/2$. To improve the accuracy of the topology method for estimating IBI, it is necessary to quantitatively analyze the effect of the above parameter assignments on method performance.

III. EVALUATION OF ASSIGNED NUMBERS USING A SIMPLIFIED MODEL

In this letter, we used a simplified model of skin displacement to evaluate the effect of the numbers assigned to RDV and FDP on the performance of the topology method. The simplified model of body displacement $d(t)$ measured using a radar system is expressed as $d(t) = d_0 + d_{\mathrm{T}}(t) + d_{\mathrm{R}}(t) + d_{\mathrm{H}}(t)$, where d_0 is the mean distance to the reflection point, and $d_{\mathrm{T}}(t)$, $d_{\mathrm{R}}(t)$, and $d_{\mathrm{H}}(t)$ are the displacements associated with body motion, respiration, and heartbeat, respectively. We assumed that $d_{\mathrm{T}}(t)$, $d_{\mathrm{R}}(t)$, and $d_{\mathrm{H}}(t)$ are all periodic functions in the local time range and have different fundamental frequencies. We also assumed that harmonics of $d_{\mathrm{H}}(t)$ higher than third order are negligible. In this case, the displacement waveform $s(t)$, obtained using an ideal bandpass filter, consists only of the fundamental wave and second harmonic of the heartbeat displacement

$$s(t) = d_{\mathrm{H}}(t) := \cos(\omega_0 t) + \alpha\cos(2\omega_0 t + \theta) \tag{1}$$

where ω_0, α, and θ are the angular frequency of the fundamental wave, the amplitude, and the initial phase of the second harmonic, respectively. We evaluated the assigned numbers with respect to the fundamental wave, so the amplitude and the initial phase of the fundamental wave can be set to 1 and 0, respectively. The amplitude of the second harmonic of the heartbeat component is often smaller than that of the fundamental wave [16], [17], so $0 \leq \alpha < 1$ is satisfied.

The six types of feature points (PK, VL, RDP, RDV, FDP, and FDV) are determined from the first-, second-, and third-order derivatives of the displacement waveform $s(t)$. The first-order derivative is expressed as

$$\dot{s}(t) = \beta_1\sin(\omega_0 t) + \beta_2\sin(2\omega_0 t + \theta) \tag{2}$$

where $\beta_1 = -\omega_0$, and $\beta_2 = -2\omega_0\alpha$. Similar to $s(t)$, $\dot{s}(t)$ is composed of the fundamental wave and second order harmonic. Similarly, the second- and third-order derivatives are expressed as follows:

$$\ddot{s}(t) = \omega_0[\beta_1\cos(\omega_0 t) + 2\beta_2\cos(2\omega_0 t + \theta)] \tag{3}$$

$$\dddot{s}(t) = -\omega_0^2[\beta_1\sin(\omega_0 t) + 4\beta_2\sin(2\omega_0 t + \theta)]. \tag{4}$$

Consider the case where $s(t)$ is represented by a fundamental wave (i.e., $\alpha = 0$). Then, $\dddot{s}(t) = -\omega_0^2\beta_1\sin(\omega_0 t) = -\omega_0^2 \cdot \dot{s}(t)$, so that $\dot{s}(t)$ and $\dddot{s}(t)$ have different signs. This indicates that among the four types of feature points satisfying $\ddot{s}(t) = 0$, only RDP and FDV appear when $s(t)$ is a fundamental wave. In other words, RDV and FDP appear as feature points only when $s(t)$ contains harmonics.

Next, consider the conditions under which the feature point RDV appears. Since $\dot{s}(t) > 0$, $\ddot{s}(t) = 0$, and $\dddot{s}(t) > 0$ are satisfied for RDV, the following are obtained using (2)–(4):

$$\beta_1\sin(\omega_0 t) + \beta_2\sin(2\omega_0 t + \theta) > 0 \tag{5}$$

$$\beta_1\cos(\omega_0 t) + 2\beta_2\cos(2\omega_0 t + \theta) = 0 \tag{6}$$

$$\beta_1\sin(\omega_0 t) + 4\beta_2\sin(2\omega_0 t + \theta) < 0. \tag{7}$$

Using (5) and (7), we obtain

$$\beta_1\sin(\omega_0 t) > 0, \quad \beta_2\sin(2\omega_0 t + \theta) < 0. \tag{8}$$

From (2), we can confirm that the fundamental and harmonic components of $\dot{s}(t)$ have different signs when RDV feature points appear. When $\alpha = 0$, $\dot{s}(t) = \beta_1\sin(\omega_0 t) > 0$ holds, RDP and RDV can be compared. The RDP is a feature point that mainly corresponds to the fundamental component, whereas the RDV is a feature point that corresponds to the harmonic component. Therefore, from (8), it is reasonable to allow the coefficients assigned to RDP and RDV to have
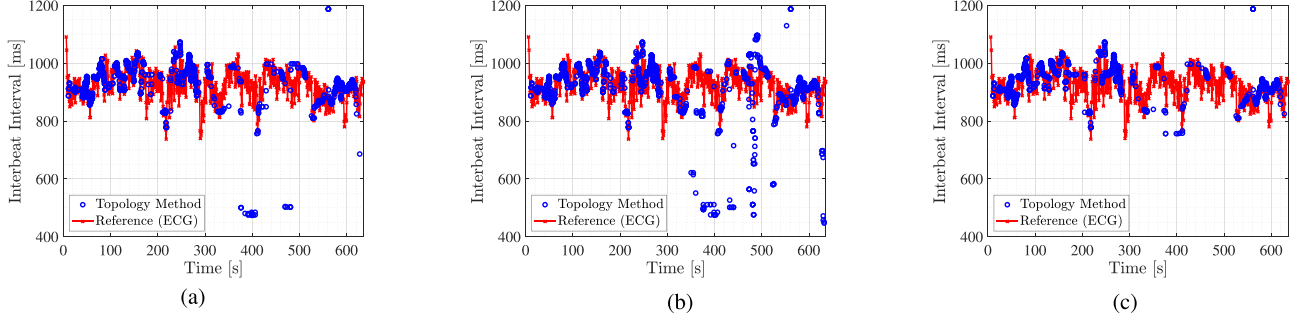
Fig. 2. IBIs estimated by applying the topology method (blue circles) to the data for subject 18 in the study of Schellenberger et al. [18]. The red lines show the reference value for the IBI obtained from an ECG [the scaling factor γ is defined in Fig. 1(b)]. (a) $\gamma = 0$. (b) $\gamma = -0.5$. (c) $\gamma = 0.625$.
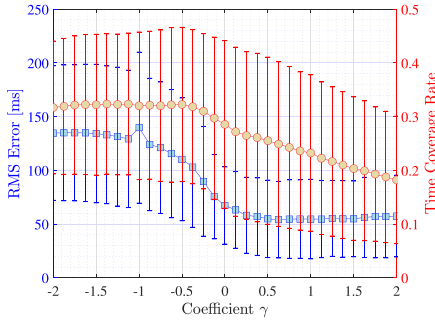

Fig. 3. RMS error and TCR for different values of γ. Data show mean $\pm$ standard deviation ($n = 21$).

different signs when both feature points corresponding to the fundamental component and the harmonic component are evaluated using topology correlation coefficients. It can be seen that the coefficients assigned to RDP and RDV should have opposite signs (i.e., $\gamma > 0$ should be satisfied).

In addition, from (5), $\beta_1^2 \sin^2(\omega_0 t) > \beta_2^2 \sin^2(2\omega_0 t + \theta)$ is obtained, and thus

$$\rho^2 < \frac{4 - 3\cos^2(\omega_0 t)}{4}, \quad \rho = \left|\frac{\beta_2}{\beta_1}\right| = 2\alpha \ (< 2) \quad (9)$$

is obtained from (6). Note that ρ and γ correspond to the coefficient ratio of the fundamental frequency and harmonics of $\dot{s}(t)$, where ρ considers only the absolute values, whereas γ considers the values with signs. Similarly, from (5) and (7), the following inequality is obtained:

$$\frac{1 + 3\cos^2(\omega_0 t)}{16} < \rho^2. \quad (10)$$

Assume that ρ^2 is uniformly distributed in (9) and (10). The time average of ρ^2, denoted as $\bar{\rho}^2$, is expressed as

$$\bar{\rho}^2 = \frac{1}{\pi} \int_\pi^{2\pi} \frac{1}{2} \left(\frac{4 - 3\cos^2(x)}{4} + \frac{1 + 3\cos^2(x)}{16}\right) dx = \left(\frac{5}{8}\right)^2 \quad (11)$$

where $x = \omega_0 t$ and $\pi \leq x < 2\pi$ satisfies because of the first inequality of (8). Considering that $\gamma > 0$, the suitable number assignment for RDV is expected to be $-j5/8$. In this case, the suitable number assignment for FDP is then $j5/8$ because FDP is the negative of RDV. Therefore, we can conclude that the optimal coefficient for RDV and FDP satisfies $\gamma = 5/8 = 0.625$, which is larger than $\gamma = 1/2$ used in the original study [11].

IV. ANALYSIS BY DATASET

A. Evaluation Specification

We evaluated the accuracy of the IBI estimate by changing the coefficient γ in the topology method and using a publicly available dataset provided by Schellenberger et al. [18]. To calculate the ordinary and topology correlation coefficients, we set the window length as $T_c = T_t = 0.5$ s. The average overlapped length is 0.33 s, so the average overlap ratio is 66%. Note that the overlapped length depends on the intervals between feature points. The thresholds c_{th} and q_{th} for the ordinary and topology correlation coefficients are set to $c_{th} = 0.7$ and $q_{th} = 0.5$, respectively. We also assumed that the IBI lies within the 0.4–1.2 s range, which corresponds to heart rates of 50–150 bpm. Complex numbers $-j\gamma$ and $j\gamma$ are assigned to feature points RDV and FDP, respectively, where the parameter γ is set to $\gamma = -2, -1.875, -1.75, \ldots, 1.75, 1.875,$ or 2.

For the evaluation, we use the dataset provided by Schellenberger et al. [18]. This dataset consists of 10-minute measurement data for each person obtained from 30 participants at rest using a 24 GHz continuous-wave radar system with a sampling frequency of 2 kHz. We resolve the DC offset by subtracting the time average value of the IQ plot. We calculate the phase using four-quadrant inverse tangent and unwrap the phase when the phase gap between consecutive samples is greater than or equal to π, and then $M \times 2\pi$ (M is a nonzero integer) is added so that the phase gap becomes less than π. To extract the heartbeat component using the topology method, a high-pass finite impulse response filter with a cutoff frequency of 0.5 Hz and a stopband attenuation of 60 dB was applied to the displacement waveform derived from the phase component of the radar signal. Note that the third harmonic of the respiration signal might affect the accuracy in estimating IBI, which needs to be addressed in future works.

The accuracy of the topology method was evaluated using the root mean square (RMS) error between the estimated IBI and a reference value obtained from an electrocardiograph (ECG) synchronized with the radar. In this study, we evaluated data pertaining to 21 of the 30 participants. Participant numbers 1–4 and 25 were excluded because no ECG data were recorded, and numbers 10, 16, 19, and 30 were excluded because their IBIs were outside the assumed 0.4–1.2 s range. We also used the time coverage rate (TCR) [19] as another evaluation criterion. The TCR is defined as $k_\varepsilon \Delta t_{TCR}/T_{all}$, where k_ε is the number of intervals that contain at least one accurately estimated point with an error of less than ε, Δt_{TCR} is the length of each time interval, and T_{all} is the total measurement time. Following Sakamoto et al. [19], we set $\varepsilon = 50$ ms and $\Delta t_{TCR} = 1.0$ s.

Table 2. Comparison Table of the RMS Error

	$\gamma = 0$ (a)	$\gamma = -0.5$ (b)	$\gamma = 0.625$ (c)	$\gamma = 0.5$ [11]
RMS error	67 ± 36 ms	110 ± 57 ms	54 ± 36 ms	55 ± 36 ms

B. Performance Evaluation

First, we show the accuracy and TCR of the topology method for participant 18 as an example. Fig. 2 shows the IBI estimated using the topology method for $\gamma = 0$, -0.5, and 0.625. Note that $\gamma = -0.5$ corresponds to the "simple assignment" introduced in the original study [11]. As shown in Fig. 2(a), the estimated values deviate more than 200 ms from the true value at times 370 s $\leq t \leq$ 410 s and 460 s $\leq t \leq$ 490 s for $\gamma = 0$, whereas Fig. 2(b) shows that the estimated values for $\gamma = -0.5$ deviate more than 200 ms from the reference value at times 350 s $\leq t \leq$ 500 s. Comparing panels (a)–(c) of Fig. 2, $\gamma = 0.625$ appears to be the best value, but this must be confirmed using data from a cohort of participants.

Fig. 3 shows the RMS error and TCR of the topology method for different values of γ. It can be seen that the RMS error for $\gamma \geq 0$ is smaller than that for $\gamma < 0$. This result supports the validity of applying opposite signs to the values of RDP and RDV (FDV and RDP), as shown in the simplified model analysis in the previous section. As a function of γ, it was also confirmed that the RMS error decreases to a minimum that is reached at approximately $\gamma = 0.625$, whereas the TCR monotonically decreases as a function of γ for $\gamma > 0$. These results indicate that $\gamma = 0.625$ is the optimal value for achieving both a low RMS error and high TCR.

From the above analysis, we confirmed that when γ is approximately 0.625, the RMS error is smallest and results in minimal exclusion of data points from the IBI estimate. Table 2 gives the comparison table of the RMS error. We also evaluate the accuracy of the topology method when γ takes a random number distributed uniformly between -2 and 2; the RMS error was 85 ± 40 ms on average with a Monte Carlo simulation with 100 trials. This finding supports the validity of the simplified model derived in Section III. Notably, the RMS error and TCR obtained using $\gamma = 0.5$ are almost the same as those obtained using $\gamma = 0.625$. This indicates the validity of the numbers $-j/2$ and $j/2$ assigned to RDV and FDP, respectively, in the original study [11].

V. CONCLUSION

In this letter, we examined the validity of complex number assignments to two types of inflection points RDV and FDP, which are feature points in the topology method for estimating the IBI using millimeter-wave radar. The validity was examined quantitatively using a simplified model of the skin displacement waveform and analysis of a publicly available dataset. We derived the optimal assignments for RDV and FDP and demonstrated that these numbers yield an IBI estimate with a low RMS error and high TCR. This suggests that although the complex numbers assigned to feature points by Sakamoto et al. [11] were empirical, they are near-optimal parameters for IBI estimation. This study is the first to show the theoretical basis of the important parameter γ in the topology method that has been applied to various radar-based heartbeat measurements.

REFERENCES

[1] C. Chen, S. Ding, and J. Wang, "Digital health for aging populations," *Nature Med.*, vol. 29, no. 7, pp. 1623–1630, 2023.

[2] D. S. Quintana, A. J. Guastella, T. Outhred, I. B. Hickie, and A. H. Kemp, "Heart rate variability is associated with emotion recognition: Direct evidence for a relationship between the autonomic nervous system and social cognition," *Int. J. Psychophysiology*, vol. 86, no. 2, pp. 168–172, 2012.

[3] M. Zhao, F. Adib, and D. Katabi, "Emotion recognition using wireless signals," *Commun. ACM*, vol. 61, no. 9, pp. 91–100, 2018.

[4] Y. Han, T. Lauteslager, T. S. Lande, and T. G. Constandinou, "UWB radar for non-contact heart rate variability monitoring and mental state classification," in *Proc. Annu. Int. Conf. IEEE Eng. Med. Biol. Soc.*, 2019, pp. 6578–6582.

[5] T. Kitagawa, K. Yamamoto, K. Endo, and T. Ohtsuki, "Multibeam Doppler sensor-based non-contact heartbeat detection using beam diversity," *IEEE Access*, vol. 10, pp. 16242–16253, 2022.

[6] M. Nosrati and N. Tavassolian, "High-accuracy heart rate variability monitoring using doppler radar based on Gaussian pulse train modeling and FTPR algorithm," *IEEE Trans. Microw. Theory Techn.*, vol. 66, no. 1, pp. 556–567, Jan. 2018.

[7] V. L. Petrović, M. M. Janković, A. V. Lupšić, V. R. Mihajlović, and J. S. Popović-Božović, "High-accuracy real-time monitoring of heart rate variability using 24GHz continuous-wave Doppler radar," *IEEE Access*, vol. 7, pp. 74721–74733, 2019.

[8] C. Ye, K. Toyoda, and T. Ohtsuki, "Blind source separation on non-contact heartbeat detection by non-negative matrix factorization algorithms," *IEEE Trans. Biomed. Eng.*, vol. 67, no. 2, pp. 482–494, Feb. 2020.

[9] F. Wang, X. Zeng, C. Wu, B. Wang, and K. J. R. Liu, "mmHRV: Contactless heart rate variability monitoring using millimeter-wave radio," *IEEE Internet Things J.*, vol. 8, no. 22, pp. 16623–16636, Nov. 2021.

[10] J. Chen, D. Zhang, Z. Wu, F. Zhou, Q. Sun, and Y. Chen, "Contactless electrocardiogram monitoring with millimeter wave radar," *IEEE Trans. Mobile Comput.*, vol. 23, no. 1, pp. 270–285, Jan. 2024.

[11] T. Sakamoto et al., "Feature-based correlation and topology similarity for interbeat interval estimation using ultrawideband radar," *IEEE Trans. Biomed. Eng.*, vol. 63, no. 4, pp. 747–757, Apr. 2016.

[12] T. Sakamoto and K. Yamashita, "Noncontact measurement of autonomic nervous system activities based on heart rate variability using ultra-wideband array radar," *IEEE J. Electromagnetics RF Microw. Med. Biol.*, vol. 4, no. 3, pp. 208–215, Sep. 2020.

[13] T. Sakamoto and T. Nakamura, "Noncontact sensing of heart rate variability from facial video using the topology algorithm," *IEICE Commun. Exp.*, vol. 11, no. 6, pp. 313–318, 2022.

[14] I. Iwata, T. Sakamoto, T. Matsumoto, and S. Hirata, "Radar-based noncontact measurement of heartbeat of humans and chimpanzees using millimeter-wave radar with topology method," *IEEE Sens. Lett.*, vol. 7, no. 11, Nov. 2023, Art. no. 7006104.

[15] Y. Tanaka, K. Sumi, I. Iwata, and T. Sakamoto, "Complex number assignment in the topology method for heartbeat interval estimation using millimeter-wave radar," 2023, *arXiv:2310.11149*.

[16] V. Nguyen, A. Q. Javaid, and M. A. Weitnauer, "Harmonic path (HAPA) algorithm for non-contact vital signs monitoring with IR-UWB radar," in *Proc. IEEE Biomed. Circuits Syst. Conf.*, 2013, pp. 146–149.

[17] Y. Xiong, Z. Peng, C. Gu, S. Li, D. Wang, and W. Zhang, "Differential enhancement method for robust and accurate heart rate monitoring via microwave vital sign sensing," *IEEE Trans. Instrum. Meas.*, vol. 69, no. 9, pp. 7108–7118, Sep. 2020.

[18] S. Schellenberger et al., "A dataset of clinically recorded radar vital signs with synchronised reference sensor signals," *Sci. Data*, vol. 7, no. 1, 2020, Art. no. 291.

[19] T. Sakamoto, S. Mitani, and T. Sato, "Noncontact monitoring of heartbeat and movements during sleep using a pair of millimeter-wave ultra-wideband radar systems," *IEICE Trans. Commun.*, vol. 104, no. 4, pp. 463–471, 2021.